African Journal of Advanced Pure and Applied Sciences (AJAPAS)
Online ISSN: 2957-644X
Volume 5, Issue 3, 2026
Page No: 432-447
Website: https://aaasjournals.com/index.php/ajapas/index
ISI 2025: 1.126 SJIFactor 2024: 6.752 معامل التأثير العربي: 1.62

Guarded Two-Time-Scale UKF and Adaptive NMPC for Voltage-Disturbance Rejection in PMSM Drives

Salah G. Abokhatwa *,
Department of Electrical and Computer Engineering, Faculty of Engineering-Garaboulli, El Mergib University, Al Khums, Libya

مرشح كالمان نوع *UKF*، ذو المقياسين الزمنيين والمزوّد بآلية حماية، مع التحكم التنبؤي غير خطي المتكيف لرفض اضطرابات الجهد في منظومات قيادة المحركات المتزامنة ذات المغناطيس الدائم

صلاح جمعه ابوخطوه *
قسم الهندسة الكهربائية والحاسوب، كلية الهندسة – القره بوللي ، جامعة المرقب، الخمس، ليبيا

*Corresponding author: sgabokhatwa@elmergib.edu.ly

Received: June 10, 2026	Accepted: September 02, 2026	Published: September 15, 2026

Abstract:
Nonlinear model predictive control (NMPC) of permanent magnet synchronous motor (PMSM) drives depends on accurate state estimates and an accurate internal motor model. Slow changes in motor parameters and rapid inverter voltage disturbances can produce similar residuals in the measured currents. Therefore, an unrestricted augmented estimator misinterprets an actuator disturbance as a change in flux linkage or load torque. This leaves the controller with a biased prediction model. This paper coordinates a guarded two-time-scale unscented Kalman filter (UKF) with adaptive constrained NMPC. A two-level test based on the dq-axis current innovations identifies and confirms an electrical event candidate before enabling disturbance cancellation. The candidate logic protects the slow flux-linkage and load-torque estimates, while a confirmed event increases the update authority for the voltage-disturbance states. The NMPC system updates the motor model while maintaining flux and load torque values at a detected electrical event. Tightened constraints ensure that some inverter capacity remains available to correct the rated voltage error without exceeding the voltage limit. Sensitivity analysis indicates that voltage and flux errors can produce similar current responses. Deterministic simulations and 30 paired Monte Carlo trials confirm the overall performance. Compared with adaptive NMPC, the proposed controller reduces the mean speed RMS error by 33.8%, the error during the disturbance interval by 79.8%, and the RMS current by 31.1%. The results show that protecting the slow states improves error attribution and that disturbance cancellation after event confirmation is the main source of improved tracking.

Keywords: permanent magnet synchronous motor; nonlinear model predictive control; unscented Kalman filter; disturbance estimation; parameter adaptation.

الملخص

يعتمد التحكم التنبؤي الغير خطي في المحركات المتزامنة ذات المغناطيس الدائم على دقة تقدير الحالات والنموذج الداخلي للمحرك. وقد تولد التغيرات البطيئة في معاملات المحرك والاضطرابات السريعة في جهد العاكس بواقي(residuals) متشابهة في التيارات المقاسة، مما قد يدفع المرشح غير المقيد إلى تفسير اضطراب الجهد على أنه تغير في الفيض أو عزم الحمل، فتتأثر دقة نموذج التنبؤ. تقترح هذه الدراسة تنسيق مرشح كالمان (UKF)غير الخطي المحمي ثنائي المقياس الزمني مع تحكم تنبؤي غير خطي تكيفي ذي قيود جهد مشددة. يستخدم المرشح اختباراً من مستويين مبنياً على ابتكار تياري المحورين لتحديد حدث كهربائي محتمل ثم تأكيده قبل تفعيل إلغاء الاضطراب. تحمي مرحلة الحدث المحتمل تقديرات الفيض وعزم الحمل البطيئة، بينما تزيد مرحلة التأكيد قدرة حالات اضطراب الجهد على التحديث. ويحدث

المتحكم نموذج التنبؤ باستخدام التقديرات المحمية، ثم يضيف جهد إلغاء محدوداً ضمن الهامش المحجوز بتشديد القيود. جرى تقييم الطريقة بمحاكاة ، وتحليل حساسية ، وثلاثين تجربة مونت كارلو مقترنة. بالمقارنة مع التحكم التكيفي، انخفض متوسط الجذر التربيعي لمتوسط مربع خطأ السرعة بنسبة 33.8%، وخطأ السرعة خلال فترات الاضطراب بنسبة 79.8%، والقيمة الفعالة للتيار بنسبة 31.1%. ارتفع جهد الذروة بنسبة 8.2%، وتبين النتائج أن حماية الحالات البطيئة تحسن إسناد الخطأ، وأن إلغاء الاضطراب بعد تأكيد الحدث هو المصدر الرئيس لتحسن التتبع.

الكلمات المفتاحية: المحرك المتزامن ذو المغناطيس الدائم؛ التحكم التنبؤي الغير خطي؛ مرشح كالمان غير الخطي؛ تقدير الاضطراب؛ تكيف المعاملات.

1. Introduction

Permanent magnet synchronous motors (PMSMs) are used in several applications because of their high torque density and fast dynamic response. Accurate control remains challenging because motor dynamics are nonlinear, machine parameters may change during operation, and the applied load torque is often unknown. Model predictive control (MPC) is well suited to these conditions because it predicts the motor response while considering control objectives and operating limits. Researchers have developed several MPC structures for PMSM drives, including finite-control-set, direct-speed, short-horizon, and continuous-control-set methods[1-3].

MPC accuracy highly depends on the prediction model. Any changes in motor parameters and load torque can reduce this accuracy. Inverter nonlinearities may also cause the applied voltage to differ from the commanded value. The predicted currents and speed may then deviate from the measured response. Robust MPC limits the effect of parameter errors [4], while online identification updates the model as machine parameters change gradually [5]. However, identifying the source of an error becomes difficult when several unknown quantities produce similar current changes. For example, an inverter-voltage error may cause the estimator to alter the magnet flux-linkage estimate even though the actual flux linkage has not changed [6]. Kalman filter methods have been used to estimate speed, flux linkage, and load torque [7], and UKF estimates have also been included in predictive PMSM control [8]. Partial-update filtering provides further protection by allowing measurements to correct only the states they can reliably support [9].

Model-free and ultra-local predictive controllers handle uncertainty differently. These methods represent unknown effects using a single disturbance estimate obtained from measured inputs and outputs [10-13]. The estimate can help compensate for parameter mismatch, inverter nonlinearities, and unmodeled dynamics. However, it cannot determine whether the mismatch comes from magnet flux linkage, load torque, or inverter-voltage error.

Existing methods usually handle fast and slow disturbances in different parts of the controller. For rapid voltage changes, the method in [14] corrects each candidate voltage vector before switching, while [15, 16] use dedicated observers for fast disturbances. They treat slower changes through the motor model. The method in [17] reduces current-prediction dependence on flux-linkage and uses a separate observer for inductance error. References [18, 19] update the motor model over longer periods as its parameters change. This separation keeps rapid electrical disturbances and gradual parameter variations in different estimation paths.

Previous studies place adaptation and compensation at different points in the PMSM control loop. In [20], a sliding-mode controller handles rotor motion, and predictive control regulates the electrical variables. Reference [21] uses a recurrent neural network to adapt the controller online. In [22], a Luenberger observer provides the compensation. The method in [23] updates the linear prediction model during operation. The control strategy used for PMSM in [24-26] estimates disturbances within or alongside the MPC calculation. These structures distribute estimation and control tasks across several elements. However, a problem arises when a single augmented nonlinear estimator uses the same current measurements to track both slow physical quantities and fast actuator disturbances. Under these conditions, a voltage event may shift the slow estimates away from their physical values.

The UKF propagates sigma points through the nonlinear motor model and does not require a Jacobian at each step [27, 28]. However, its measurement update still relies on the innovation. If the same current residual can be explained by either slow parameter changes or a fast voltage disturbance, the filter may update the wrong state. The method in [29] uses a normalized innovation squared (NIS) threshold to pause parameter updates during a disturbance. The two-stage UKF in [30] estimates the plant states and an unknown input separately. Once estimated, the disturbance can be included in the voltage command calculated by MPC [31]. This correction uses part of the inverter's voltage capacity. By tightening the nominal voltage constraint, the NMPC keeps its command below the inverter limit and leaves some available voltage for disturbance correction [32, 33]. A single-event decision protects the slow estimates and determines when the controller can use this reserved voltage.

An isolated current residual is not sufficient to confirm a change in the inverter voltage command. The proposed guard therefore separates initial detection from confirmation. Crossing the lower threshold protects the most recent reliable flux-linkage and load-torque estimates, while the UKF continues to update the voltage-disturbance states. The disturbance is confirmed only when the residual remains high for the required number of samples or exceeds the higher threshold. The filter then allows the voltage-disturbance estimates to respond faster, and the adaptive NMPC adds a bounded correction using the inverter margin reserved by the tightened voltage constraint. The protected slow estimates remain in the NMPC model throughout the event.

The main contribution is a two-stage decision shared by the estimator and the controller. When a voltage disturbance is first detected, the estimator holds the slow physical estimates and keeps cancellation inactive, preventing a single unusual residual from triggering a control action. Once the event is confirmed, the controller compensates for the estimated disturbance while keeping the applied voltage within the inverter limit.

The proposed method is evaluated using estimator replay, controller ablation, local sensitivity analysis, and paired Monte Carlo simulations. The estimator replay compares an unguarded augmented UKF, an NIS-scheduled augmented UKF, and the proposed guarded two-time-scale UKF. Tracking performance is reported using speed RMSE, speed IAE, and disturbance-window RMSE, while paired statistical tests examine whether the observed differences remain consistent across trials.

2. PMSM Model and Estimation Problem

Figure 1 shows the overall PMSM drive considered in this study. The guarded adaptive UKF estimates the motor states and disturbances, while the NMPC uses these estimates to calculate the voltage commands.

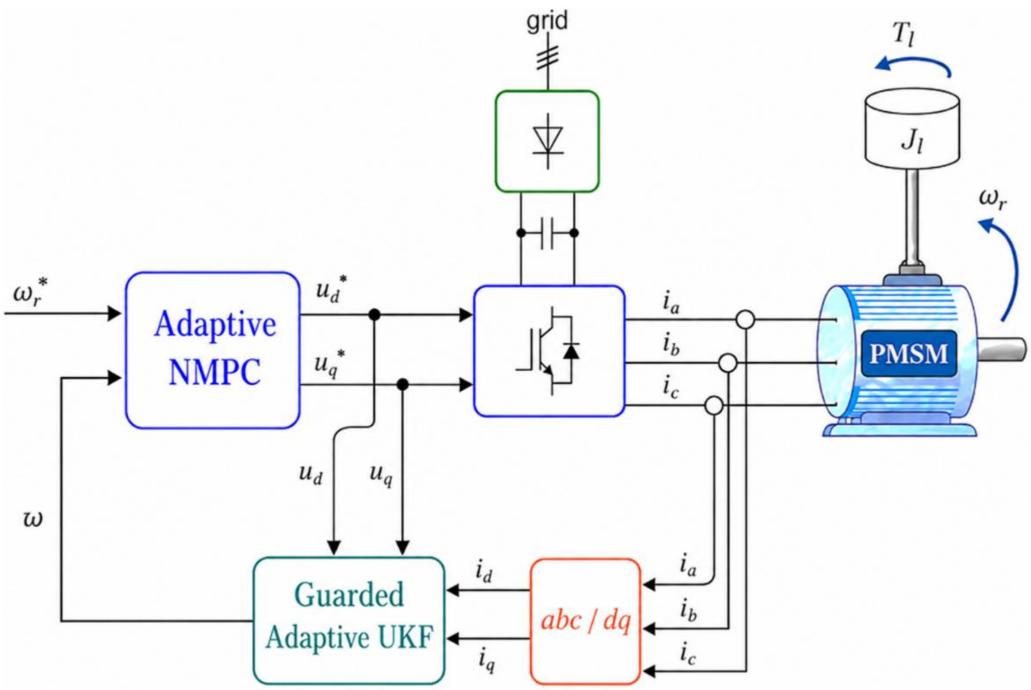

Figure 1. Overall structure of the proposed guarded adaptive UKF and NMPC scheme for the PMSM drive.

2.1 Nonlinear dq model

The PMSM is represented in the rotor-oriented dq frame [34]. Mechanical speed is ω, Electrical speed is $p\omega$, and p denotes the number of pole pairs. The commanded voltage is $u = \left[v_d, v_q\right]^T$. A matched disturbance $d_v = \left[d_{v_d}, d_{v_q}\right]^T$ represents inverter nonlinearity, voltage loss, and other errors that enter the plant through the same channels as the commanded voltage. The continuous-time dynamics are

$$\begin{aligned} i_d &= \frac{v_d + d_{v_d} - R_s i_d + p\omega L_q i_q}{L_d}, \\ i_q &= \frac{v_q + d_{v_q} - R_s i_q - p\omega\left(L_d i_d + \psi_f\right)}{L_q}, \\ \dot{\omega} &= \frac{T_e - T_L - B\omega}{J}. \end{aligned} \tag{1}$$

The electromagnetic torque is

$$T_e = \frac{3}{2} p\left[\psi_f i_q + \left(L_d - L_q\right) i_d i_q\right]. \tag{2}$$

Here, R_s, L_d, and L_q are the stator resistance and dq inductances, ψ_f is the magnet flux linkage, J and B are the mechanical coefficients, and T_L is the load torque. The measured output is $y_k = \left[i_{d,k}, i_{q,k}, \omega_k\right]^T + n_k$, where n_k is zero-mean measurement noise with covariance R. The guard developed in Section 3 uses only the current-innovation subvector; a change in the speed reference is not, by itself, evidence of an electrical event. A fourth-order Runge-Kutta (RK4) map yields the discrete process model [35].

$$\begin{aligned} x_{k+1} &= F_{RK4}\left(x_k, u_k + d_{v,k}, \psi_{f,k}, T_{L,k}\right) + w_k, \\ y_k &= x_k + n_k. \end{aligned} \tag{3}$$

The term w_k represents process and model uncertainty. The plant and the controller use the same continuous equations but different numerical integration settings, as specified in the simulation design.

2.2 Slow and fast augmented states

The UKF state is

$$\xi = \left[i_d,\ i_q,\ \omega,\ \psi_f,\ T_L,\ d_{v_d},\ d_{v_q}\right]^T. \tag{4}$$

The current components describe fast electrical dynamics. Magnetic flux linkage and load torque typically evolve more slowly, whereas an inverter-voltage disturbance may change within a single electrical event. Around a nearly constant-speed operating point, the leading q-axis perturbation is

$$L_q\, \delta i_q \approx \delta d_{v_q} - p\omega\, \delta\psi_f. \tag{5}$$

Equation (5) shows that the same current increase can result from either a positive voltage disturbance or a decrease in magnet flux linkage. Therefore, the current measurement gives the UKF no clear basis for distinguishing between these two causes. The guard uses the rate at which the residual develops to resolve this ambiguity. When a large residual appears quickly and passes the event test, the filter treats it as a possible electrical disturbance. It then holds the flux-linkage and load-torque corrections and uses the current residual to update the voltage-disturbance states.

3. Guarded Two-Time-Scale UKF

3.1 UKF recursion and event evidence

The estimator uses a scaled UKF with fixed sigma-point parameters [27, 28]. It propagates the sigma points through the augmented nonlinear model and then computes the predicted state and covariance from the weighted moments of the sigma points. The measurement update is

$$\begin{aligned} \hat{\xi}_k^- &= \textstyle\sum_i W_i^{(m)} \chi_{i,k}^-, \\ P_k^- &= \textstyle\sum_i W_i^{(c)} \tilde{\chi}_{i,k}^- \tilde{\chi}_{i,k}^{-T} + Q_k, \\ \nu_k &= y_k - \hat{y}_k^-, \qquad K_k = P_{\xi y,k} S_k^{-1}, \\ \hat{\xi}_k^+ &= \hat{\xi}_k^- + K_k \nu_k, \\ P_k^+ &= P_k^- - K_k S_k K_k^T. \end{aligned} \tag{6}$$

Here, $\hat{y}_k^-$ is the weighted mean of the transformed measurement sigma points, S_k is their predicted covariance including the measurement covariance R, and $P_{\xi y,k}$ is the predicted state-measurement cross-covariance.

The base process covariance Q_0 and measurement covariance R remain fixed. The effective process covariance also includes the operating-point-dependent term defined in Section 3.2. When the guard confirms an electrical event, it adds a prescribed variance only to the two voltage-disturbance states. As a result, their predicted uncertainty increases, so the current innovation updates the disturbance more quickly. No innovation-based adaptation is applied to Q_0 or R.

Only the current channels activate the guard. Let $\nu_{e,k} = \left[\nu_{i_d,k}, \nu_{i_q,k}\right]^T$ and let $S_{e,k}$ denote the corresponding innovation-covariance block. The guard uses the normalized innovation squared (NIS), which measures the innovation relative to its predicted covariance [29, 36]. The current-only NIS is calculated as

$$\gamma_k = \nu_{e,k}^T S_{e,k}^{-1} \nu_{e,k}. \tag{7}$$

The event logic uses two thresholds. An ordinary event must exceed γ_o for N_c consecutive samples, whereas an innovation above the higher threshold γ_e is confirmed immediately:

$$c_k = \mathbb{I}\left[(\gamma_k > \gamma_e) \vee \left(\min_{0 \le r < N_c} \gamma_{k-r} > \gamma_o\right)\right], \qquad 0 < \gamma_o < \gamma_e. \tag{8}$$

Here, $\mathbb{I}[\cdot]$ is the indicator function and c_k is the binary confirmation signal. The lower threshold γ_o requires the current NIS to remain high for N_c samples. The higher threshold γ_e confirms an event based on the current sample alone. An isolated NIS value between the two thresholds does not trigger cancellation, which limits the effect of an occasional noise spike.

3.2 Process-covariance contribution from unestimated parameters

The simulated plant includes uncertainty in L_d, L_q, R_s, J, and B, but these five quantities are not included in the UKF state. We account for their local one-step effect through a covariance term. Let $\vartheta = [L_d, L_q, R_s, J, B]^T$ and let $G_{\vartheta,k} \in \mathbb{R}^{3\times 5}$ contain the sensitivity of the RK4 state map to these parameters. Its jth column is evaluated about the nominal parameter vector $\bar{\vartheta}$ using the centered difference

$$[G_{\vartheta,k}]_{:,j} \approx \frac{F_{RK4}(x_k, u_k; \bar{\vartheta} + h_j e_j) - F_{RK4}(x_k, u_k; \bar{\vartheta} - h_j e_j)}{2h_j},$$

where h_j is the finite-difference step and e_j is the jth unit vector. For independent parameters distributed as $\vartheta_j \sim \mathcal{U}[\bar{\vartheta}_j - a_j, \bar{\vartheta}_j + a_j]$, the half-width a_j gives $\mathrm{var}(\vartheta_j) = a_j^2/3$. Using the first-order law of uncertainty propagation [37], the corresponding one-step covariance is

$$Q_{\mathrm{model},k} = G_{\vartheta,k}\, \mathrm{diag}\left(\frac{a_1^2}{3}, \dots, \frac{a_5^2}{3}\right) G_{\vartheta,k}^T. \tag{9}$$

Equation (9) provides a local approximation of how uncertainty in the unestimated parameters affects the one-step state prediction. The 3×3 result is inserted into the electrical and mechanical state block of the augmented process covariance; the rows and columns for ψ_f, T_L, and d_v receive no contribution from this term. Each Monte Carlo run uses a fixed parameter realization drawn at the start of the run, whereas the UKF receives only $\bar{\vartheta}$ and the prescribed uncertainty widths. Thus, $Q_{\mathrm{model},k}$ represents the effect of unknown but fixed parameters and does not imply that the plant parameters are redrawn at every sample.

3.3 Guarded slow-fast update

The guard does not determine the physical source of a residual from current data alone. Instead, it uses the expected rate of change for each state. A slowly developing residual remains available for the flux-linkage and load-torque updates. A large or persistent current residual triggers an electrical-event candidate, and the filter then sets the innovation corrections for ψ_f and T_L to zero. The voltage-disturbance states continue to update. Cancellation remains disabled until the event satisfies (8).

After confirmation, the slow-state corrections remain blocked, and the added disturbance-state variance lets $\hat{d}_v$ follow the event more quickly. This operation changes which state means can receive the innovation; it does not remove the voltage disturbance from the motor-state prediction. The estimated currents and speed still evolve through the full plant model, including $\hat{d}_v$.

Outside an active or retained-candidate interval, the disturbance mean and covariance decay together:

$$\begin{aligned} \hat{d}_{v,k}^{+} &\leftarrow \lambda_d \hat{d}_{v,k}^{+}, \\ P_k^{+} &\leftarrow A_\lambda P_k^{+} A_\lambda^T, \\ A_\lambda &= \mathrm{diag}(I_5, \lambda_d I_2), \qquad 0 < \lambda_d < 1. \end{aligned} \tag{10}$$

When the confirmation signal in (8) becomes one, the state machine sets the active-mode flag g_k to one. This latched flag, rather than a single-threshold result, enables the cancellation command in (15).

The confirmed mode remains active for at least the prescribed dwell time. It is released when both the current NIS and the magnitude of $\hat{d}_v$ fall below their respective release levels. A timeout ends an unusually long activation, and a cooldown interval prevents an immediate ordinary-threshold retrigger. When no candidate or confirmed event is present, (10) sets the inactive disturbance estimate and its covariance to zero.

The current-innovation test moves the method through the normal, candidate, confirmed, and recovery stages. Table 1 summarizes the corresponding actions of the UKF and NMPC at each stage. Figure 2 presents the overall estimator–controller architecture.

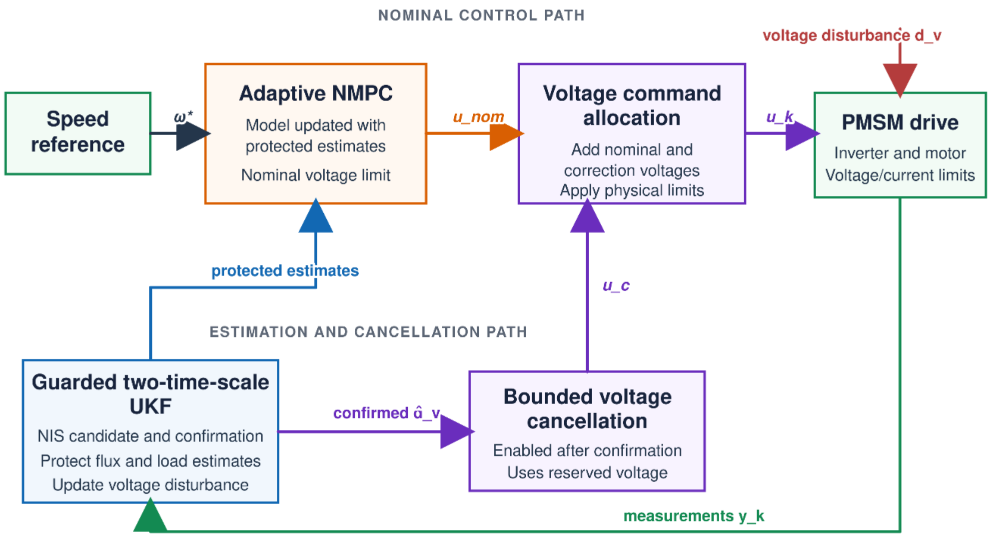

Figure 2. Proposed guarded UKF–adaptive NMPC architecture.

Algorithm 1 summarizes the guarded UKF update at each sampling instant.

Algorithm 1. Guarded two-time-scale UKF update

Step 1: Propagate the sigma points with $Q_0 + Q_{\mathrm{model},k}$ and calculate the predicted state, covariance, current innovation, and innovation covariance.
Step 2: Calculate the current-only NIS and evaluate the confirmation signal in (8).
Step 3: At the first ordinary crossing, retain the predicted values of ψ_f and T_L, continue the voltage-disturbance update, and keep cancellation disabled.
Step 4: After confirmation, set the active-mode flag, keep the two slow-state innovation corrections at zero, and add the event variance to the d- and q-axis disturbance block.
Step 5: After the minimum dwell, release the event when both release tests are satisfied; otherwise, apply the timeout and cooldown rules.
Step 6: In normal mode, apply the inactive-state decay in (10) and return the state, parameter, disturbance, and mode estimates.

Table 1. Event-governed estimator and controller decision sequence

Mode	Evidence and decision	Estimator action	Controller action
Normal	The current NIS is below both event conditions.	Update all states; apply the inactive decay in (10).	Set $u_{c,k} = 0$.
Candidate	The ordinary threshold is crossed once, but the confirmation condition in (8) is not yet satisfied.	Hold $\hat{\psi}_f$ and $\hat{T}_L$; retain the fast-state update.	Keep $u_{c,k} = 0$.
Confirmed	The confirmation signal is set by an emergency crossing or by the required consecutive ordinary crossings.	Keep the slow corrections at zero, add the event variance to the disturbance block, and set active mode.	Apply the limited cancellation term in (15).
Recovery	The dwell time has passed, and both release tests are met; the timeout handles a long event.	Restore normal slow-state correction and decay the inactive d_v states.	Disable cancellation and begin the cooldown interval.

4. Adaptive NMPC and Command Allocation

4.1 Online model update and optimization problem

The controller augments the physical state with an integral state, giving $z = \left[i_d, i_q, \omega, \zeta\right]^T$. The integral state accumulates speed error within the bounds $\zeta_{\min}$ and $\zeta_{\max}$:

$$\zeta_{k+1} = \mathrm{sat}_{[\zeta_{\min},\zeta_{\max}]}[\zeta_k + T_s(\omega_k^* - \hat{\omega}_k)]. \tag{11}$$

The estimated flux linkage and load torque update the prediction model and its equilibrium target. For $i_d^* = 0$,

$$\begin{aligned} i_q^* &= \frac{B\omega^* + \hat{T}_L}{1.5p\hat{\psi}_f}, \\ u_d^* &= -p\omega^* L_q i_q^*, \\ u_q^* &= R_s i_q^* + p\omega^* \hat{\psi}_f. \end{aligned} \tag{12}$$

At each sample, define $e_{z,j} = z_j - z^*$ and $e_{u,j} = u_j - u^*$. To avoid confusion with the UKF process covariance, Q_z denotes the NMPC state-weighting matrix. Following the standard finite-horizon NMPC formulation [38], the optimization problem is

$$\begin{aligned} \ell_j &= \| e_{z,j} \|_{Q_z}^2 + \| e_{u,j} \|_{R_u}^2 + \| \Delta u_j \|_{S_u}^2 + \rho_\epsilon \epsilon_j^2, \\ \min_{U,\epsilon} J_N &= \textstyle\sum_{j=0}^{N_p-1} \ell_j + \| e_{z,N_p} \|_{Q_f}^2. \end{aligned} \tag{13}$$

The predicted dynamics and feasible set are

$$\begin{aligned} z_{j+1} &= F_a\left(z_j, u_j, \omega^*; \hat{\psi}_{f,k}, \hat{T}_{L,k}\right), \\ \| u_j \|_2 &\le V_{\mathrm{nom}}, \qquad \| \Delta u_j \|_2 \le \Delta U_{\max}, \\ \| i_{dq,j+1} \|_2^2 &\le I_{\mathrm{nom}}^2 + \epsilon_j, \qquad \epsilon_j \ge 0. \end{aligned} \tag{14}$$

The terminal matrix Q_f is obtained from the discrete Riccati equation of the linearized augmented model [38]. A strongly penalized slack variable softens only the current constraint.

4.2 Confirmed cancellation and constraint reserve

Let V_{phys} denote the inverter voltage limit. Following the constraint-tightening principle [32, 33], the nominal NMPC uses the smaller bound V_{nom}, leaving $V_{\mathrm{res}} = V_{\mathrm{phys}} - V_{\mathrm{nom}}$ available for corrective action. After the guard confirms an event, the estimated voltage disturbance is included as a bounded correction to the nominal MPC command [31]. If $\mathcal{S}_r(\cdot)$ limits a vector to magnitude r, the cancellation command is

$$u_{c,k} = \begin{cases} -\mathcal{S}_{V_{\mathrm{res}}}\left(\hat{d}_{v,k}\right), & g_k = 1, \\ 0, & g_k = 0. \end{cases} \tag{15}$$

The final command first combines the NMPC and cancellation terms. The physical magnitude and slew-rate projections are then applied:

$$\bar{u}_k = \mathcal{S}_{V_{\mathrm{phys}}}\left(u_{\mathrm{nom},k} + u_{c,k}\right), \qquad u_k = \mathcal{R}_{\Delta U_{\max}}(\bar{u}_k; u_{k-1}), \qquad V_{\mathrm{nom}} + V_{\mathrm{res}} = V_{\mathrm{phys}}. \tag{16}$$

The operator $\mathcal{R}_{\Delta U_{\max}}(\bar{u}_k, u_{k-1})$ limits the change in the command relative to the previous input. The reserve does not alter $\hat{d}_{v,k}$; it only prevents the nominal optimizer from using the voltage required for a confirmed correction. The construction respects the stated physical limit in the tested simulations, but it does not provide a tube-MPC or invariant-set guarantee.

Algorithm 2 summarizes the adaptive NMPC calculation and final voltage-command allocation.

Algorithm 2. Adaptive NMPC with confirmed disturbance cancellation

Step 1: Read the motor-state estimate, protected slow estimates, voltage-disturbance estimate, confirmation flag, and previous command.

Step 2: Update the prediction model and equilibrium target, then solve (13)-(14) with the nominal voltage bound.

Step 3: If $g_k = 1$, calculate the cancellation term from (15); otherwise, set $u_{c,k} = 0$.

Step 4: Form the final voltage command and apply the magnitude and slew limits in (16).

Step 5: Apply the command and warm-start the next optimization with the shifted solution.

The candidate mode protects the slow estimates while the guard collects a second sample, but it cannot change the applied voltage. Only the confirmed mode passes $\hat{d}_{v,k}$ to the cancellation path. This ordering prevents a single moderate residual from reaching the voltage command.

5.1 Plant, events, and numerical settings

In this simulation, the NMPC problem is formulated in CasADi [39] and solved using Ipopt [40]. The simulation lasts 3 s. After startup, the speed reference takes the values 80, 190, and 130 rad/s. The magnet flux linkage begins a 22% exponential decrease at 0.75 s. Load torque changes from 0.10 to 0.75 N·m at 1.10 s and then to -0.25 N·m at 2.30 s; stator resistance increases by 55% at 1.50 s. The plant also receives three matched voltage disturbances: $[18, -14]^T$ V from 1.40 to 1.55 s, a 35-Hz ripple with d- and q-axis amplitudes of 10 and 8 V from 1.72 to 1.92 s, and $[-20,16]^T$ V from 2.48 to 2.63 s. All controllers use the same measurement-noise realization. Table 2 lists the nominal plant, estimator, and controller parameters used in simulation.

Table 2. Nominal plant, estimator, and controller settings used in simulation

Quantity	Tested value	Quantity	Tested value
R_s, L_d, L_q	0.10 Ω, 1.5 mH, 1.8 mH	ψ_f, J	0.10 Wb, 8×10^{-3} kg·m²
B, pole pairs	8×10−4 N·m·s, 4	Sample time; RK4 substeps (plant/controller)	1 ms; 5/1
Prediction horizon N_p	15	Integral-state bounds	$[-80,80]$
Q_z	$\mathrm{diag}(0.8,0.8,22,30)$	R_u, S_u, ρ_ε	$2 \times 10^{-3} I_2$, $3 \times 10^{-2} I_2$, 2000
Physical voltage/current	160 V / 45 A	Nominal voltage/current	128 V / 40 A
Voltage reserve	32 V	Slew limit	45 V/sample
Ordinary/emergency NIS gates	25 / 500	Ordinary confirmation	2 samples
Dwell/timeout/cooldown	20 / 300 / 100 ms	Release levels	NIS 1.0 / disturbance 1.2 V
Active disturbance variance	0.5 V²/sample	Inactive decay λ_d	0.35
Terminal matrix	DARE solution	Slowest terminal-pole magnitude	0.998833

Three controllers are tested side by side under the same conditions. Fixed NMPC uses the nominal motor parameters. Adaptive NMPC updates flux linkage and load torque with an unrestricted augmented UKF but does not cancel voltage disturbances or reserve voltage for correction. The proposed controller protects the slow estimates during electrical events, cancels confirmed voltage disturbances, and reserves voltage for this action. If the solver cannot find a feasible solution, the controller applies the last feasible command.

5.2 Ablations, sensitivity study, and Monte Carlo design

The estimator replay starts with an unrestricted joint UKF. Four cumulative variants then add event-based variance scheduling, slow-mean protection, covariance conditioning, and the full activation lifecycle. Each variant processes the same stored measurements. A separate controller ablation compares adaptive NMPC (A), tightening only (T), cancellation only (C), and cancellation with tightening (C+T), while the guarded UKF remains unchanged.

Local identifiability is examined by varying the rise times of a flux-linkage change and a q-axis voltage disturbance. Let Y collect the simulated current samples, and let A_ψ and A_v denote the corresponding change amplitudes. The sensitivity matrix is $S = [\partial Y / \partial A_\psi, \ \partial Y / \partial A_v]$. Normalize its columns before computing the condition number and absolute correlation. A large condition number, or a correlation close to one, means that the two current signatures provide little independent information.

The statistical study uses 30 paired Monte Carlo runs with seeds 200-229. Motor parameters vary independently within $\pm 20\%$ of their nominal values, the flux scale within $\pm 10\%$, load and disturbance amplitudes within

$\pm 20\%$, and noise scales within $\pm 25\%$. The adaptive and proposed controllers receive the same parameter and noise realization for each seed. Their paired difference therefore removes the variation shared within that run.

5.3 Evaluation measures and statistical interpretation

Tracking, estimation, and covariance consistency are reported separately. For a scalar state z, the estimation error is $e_{z,k} = z_k - \hat{z}_k$; the speed-tracking error is $e_{\omega,k} = \omega_k^* - \omega_k$. Over the sample set $\mathcal{K}$, the root-mean-square error (RMSE) and integral absolute error (IAE) are

$$\mathrm{RMSE}_z(\mathcal{K}) = \sqrt{\frac{1}{|\mathcal{K}|}\sum_{k\in\mathcal{K}} e_{z,k}^2}, \qquad \mathrm{IAE}_\omega(\mathcal{K}) = T_s \sum_{k\in\mathcal{K}} |e_{\omega,k}|. \tag{17}$$

The full-record tracking set begins 0.25 seconds after startup. The disturbance set contains only the three input voltage event windows. Therefore, the root mean square error (RMSE) for the disturbance window is a velocity-tracking measure evaluated only during these windows; it is not a voltage-estimation measure. The RMS uses its own estimation errors to correlate flux, load torque, and voltage disturbance.

For covariance-consistency analysis, the normalized innovation squared (NIS) and normalized estimation error squared (NEES) are compared with their corresponding chi-square confidence intervals [36]. The NIS compares the measured current residual with the covariance predicted by the UKF. It is the same statistic used by the guard in (7):

$$\mathrm{NIS}_k = \nu_{e,k}^T S_{e,k}^{-1} \nu_{e,k} = \gamma_k. \tag{18}$$

For samples that exclude injected events and load transitions, a consistent two-current model gives $\mathrm{NIS}_k \sim \chi_2^2$ and $E[\mathrm{NIS}_k] = 2$. The clean-sample mean and the percentage inside the central 95% χ_2^2 interval are reported. The event thresholds in Table 2 are much higher than this consistency interval because they are intended to detect actuator events, not ordinary stochastic variation.

The NEES applies the same consistency test to the state-estimation error:

$$\mathrm{NEES}_k = \tilde{x}_k^T P_{x,k}^{-1} \tilde{x}_k, \qquad \tilde{x}_k = x_k - \hat{x}_k. \tag{19}$$

For a state block of dimension n_x, consistency gives $E[\mathrm{NEES}_k] = n_x$ and approximately 95% coverage in the corresponding central χ^2 interval. The replay ablation uses all seven augmented states. The Monte Carlo summary uses only $[i_d, i_q, \omega]^T$. NEES requires the true state, so it can be computed here from simulation, but an experiment would require an independent reference.

For each Monte Carlo metric, $d_r = m_{A,r} - m_{P,r}$ compares adaptive and proposed control within each run r. The 95% confidence interval for the mean paired difference is

$$\bar{d} \pm t_{0.975,29} \frac{s_d}{\sqrt{30}}. \tag{20}$$

For an error or current metric, a positive interval favors the proposed controller. Treat peak voltage separately because a higher value represents a control-effort cost.

6. Results and Discussion

6.1 Deterministic NMPC comparison

Figure 3 shows the speed responses and corresponding tracking errors for the three controllers. Although the speed trajectories in the upper panel appear similar, the lower panel shows clear differences across the three voltage events. Fixed and adaptive NMPC produce larger error excursions and take longer to recover. After the guard confirms each event, the proposed controller uses the estimated disturbance to correct the voltage command. This action reduces the tracking error and returns the speed to its reference more quickly, demonstrating the benefit of active disturbance cancellation.

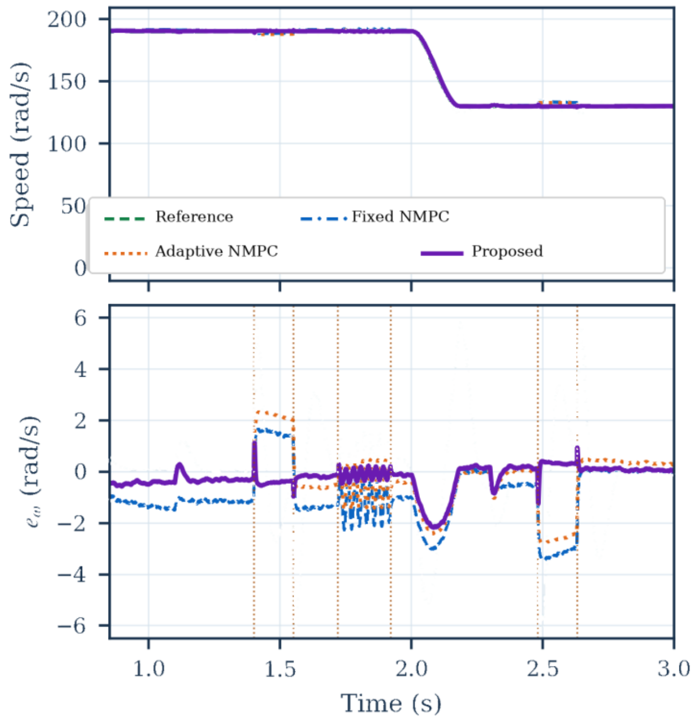

Figure 3: Deterministic NMPC comparison. Top: speed trajectories. Bottom: speed-tracking error for fixed NMPC, adaptive NMPC, and the proposed controller. Vertical dotted lines mark the voltage-disturbance boundaries.

Table 3. Deterministic NMPC performance and control effort

Controller	Speed RMSE (rad/s)	Speed IAE (rad)	Disturbance-window RMSE (rad/s)	RMS current (A)	Peak current (A)	Peak voltage (V)
Fixed NMPC	1.4051	2.9579	1.6968	5.3659	14.377	94.44
Adaptive NMPC	1.1441	2.1615	1.4613	4.4689	15.977	90.78
Proposed	0.7528	1.2539	0.2911	3.0752	15.107	98.87

The controllers differ most clearly during the three voltage disturbances shown in Figure 3. With adaptive NMPC, the speed RMSE reaches 1.5385 rad/s during the first voltage step and 1.8165 rad/s during the second. The proposed controller lowers these values to 0.3571 and 0.2777 rad/s, respectively. A similar reduction also appears during the ripple interval, where the RMSE decreases from 0.7348 to 0.2113 rad/s. Table 3 shows that the proposed correction improves tracking during both abrupt and oscillatory voltage disturbances. The reduction during the ripple interval indicates that the cancellation is effective for oscillatory disturbances and sharp voltage changes. The proposed controller also has the lowest tracking and disturbance errors. The peak voltage is higher than that of adaptive NMPC because the controller uses the reserved voltage margin to oppose the disturbance. The peak value remains below the inverter limit, confirming that the additional correction respects the physical voltage constraint.

Figure 4 shows the estimated d- and q-axis voltage disturbances and the guard state over the full record. Away from the three injected events, the adaptive and guarded estimates remain close to zero. Each event is confirmed after 1 ms, and active mode covers 99.4% of the injected-event samples. All three events leave active mode through the normal release rule, with a mean release delay of 2.33 ms and a maximum of 3 ms. No activation occurs outside the prescribed voltage-event windows. The largest cancellation vector is 25.80 V, below the 32-V reserve. Flux-linkage and load-torque RMSE are 2.42×10^{-4} Wb and 0.0845 N·m, respectively.

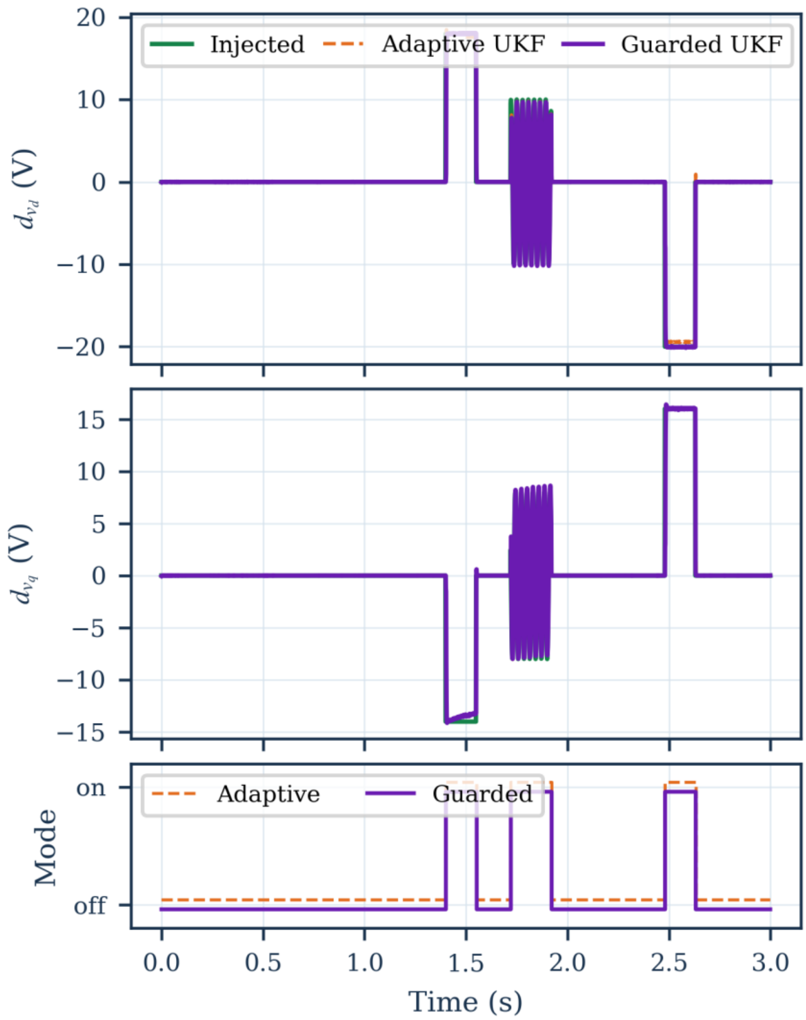

Figure 4: Full-record d- and q-axis voltage-disturbance estimates and guarded-mode activity. Cancellation is enabled only after the current-innovation test confirms an event.

6.2 Estimator and controller ablations

In this replay, M accounts for almost all of the measured improvement. Adding C changes the post-event voltage-disturbance RMSE from 0.740 to 0.737 V. This 0.003 V difference is too small to appear in Figure 5, and the G result overlaps it. The three cases are therefore shown by one bar, with the exact values given in Table 4. The selected event neither produces large covariance growth nor keeps the active mode engaged for long, so it does not test the additional safeguards in C and G. Speed RMSE also cannot settle the attribution question. Cancellation may keep the speed close to its reference even when the flux-linkage or load-torque estimate is biased. The state errors, NIS, NEES, and active-mode duration are used to detect this problem.

For the selected event, M has already achieved the final replay accuracy. Adding C only changes the post-event voltage-disturbance RMSE by 0.003 V, and G doesn't make any additional difference at the reported precision. Since the three bars would overlap in Figure 5, display only one, while Table 4 provides the exact values. This result means that the covariance and timing safeguards were not called upon during this replay. It does not show how they would behave during a longer event or greater covariance growth.

Speed RMSE does not reliably indicate this estimation issue. Once cancellation is active, the controller can maintain the speed response even if the flux-linkage or load-torque estimate has shifted. To identify that case, you need the state errors, NIS, NEES, and active-mode duration.

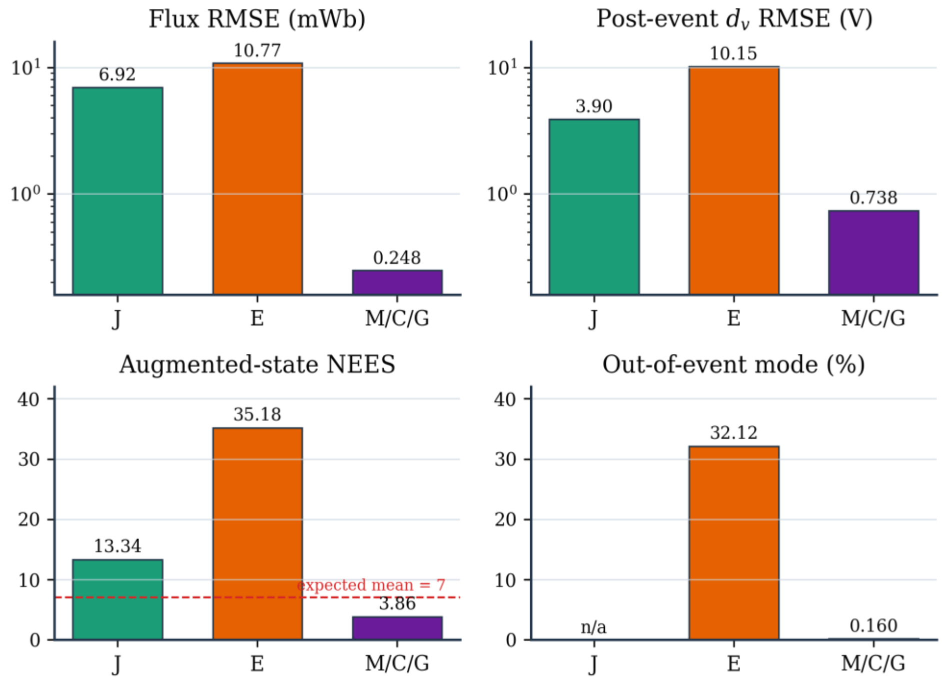

Figure 5: Condensed estimator replay ablation. J: unrestricted joint UKF; E: NIS scheduling; M/C/G: the slow-mean, covariance-conditioned, and complete-guard stages grouped because their results are equal to plot precision.

Table 4. Exact estimator-focused replay results

Variant	Flux RMSE (mWb)	Peak event-window flux error (mWb)	Post-event d_v RMSE (V)	Full-state NEES	Activation outside events (%)
Joint UKF (J)	6.921	14.215	3.899	13.343	n/a
NIS scheduling (E)	10.765	20.847	10.148	35.180	32.12
Slow-mean protection (M)	0.248	1.189	0.740	3.858	0.16
Mean/covariance (C)	0.248	1.189	0.737	3.867	0.16
Complete guard (G)	0.248	1.189	0.737	3.867	0.16

As listed in Table 4, most of the estimator's improvement comes from slow disturbance protection (M), which, compared to E, decreases the flux RMSE from 10.765 to 0.248 mWb and reduces the full-state NEES from 35.180 to 3.858. C changes the voltage disturbance RMSE by only 0.003 V, and G provides no improvement in this replay. Because the event does not stress the covariance or timing limits, the separate benefits of C and G remain untested. Disturbance attribution is therefore evaluated using the state errors, NIS, NEES, and active-mode duration, rather than speed RMSE alone.

The hardest case occurs when the flux-linkage and voltage-disturbance rise times are nearly equal, at 38.5 and 37.3 ms, respectively. At this point, the sensitivity columns have a correlation of 0.999983, and the condition number rises to 345.368, the highest among the 675 cases. The current response then contains little information to separate the two errors. This result supports the assumed time-scale difference between a fast voltage disturbance and a slower parameter change.

Figure 6 shows that cancellation improves tracking. Tightening alone has little effect because the nominal command does not reach its boundary. Its role is to reserve voltage for cancellation and to keep the final command within the inverter limit.

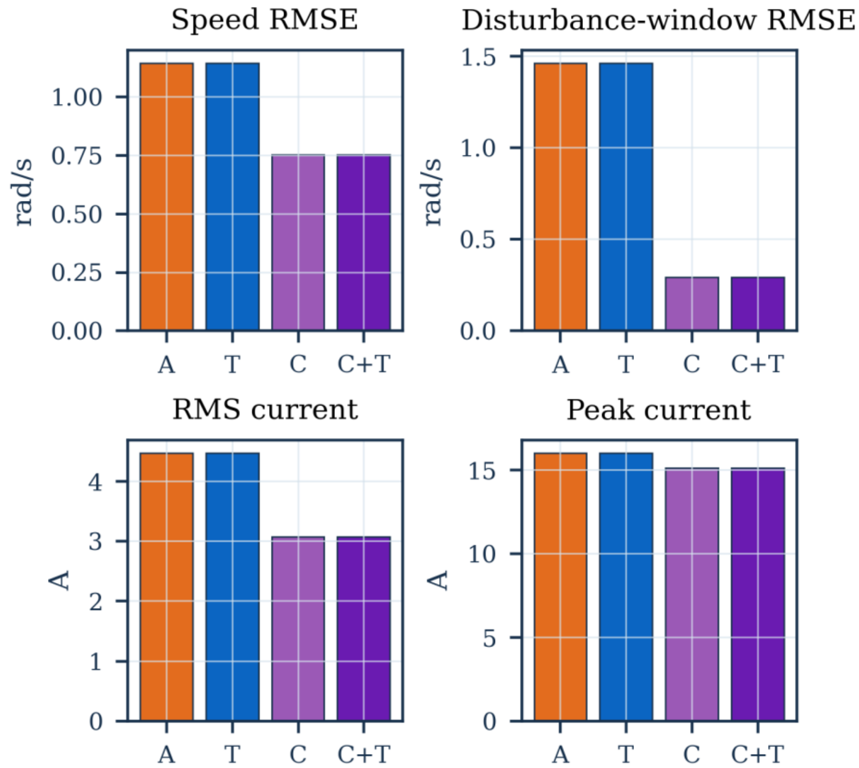

Figure 6: Controller ablation. A: adaptive NMPC; T: tightening only; C: cancellation only; C+T: cancellation with tightening.

6.3 Paired Monte Carlo results

Table 5 reports the 30 paired runs. The 95% confidence intervals for the adaptive-minus-proposed differences remain above zero for all error and current metrics. Mean speed RMSE decreases by 33.8%, disturbance-window RMSE by 79.8%, and RMS current by 31.1%. Peak voltage increases by 8.2%, reflecting the extra control action applied during confirmed events.

Table 5. Thirty-run paired adaptive-to-proposed Monte Carlo summary

Metric	Adaptive mean ± SD	Proposed mean ± SD	Paired difference [95% CI]	Wins
Speed RMSE (rad/s)	1.15 ± 0.09	0.76 ± 0.07	0.389 [0.352, 0.426]	30/30
Speed IAE (rad)	2.17 ± 0.16	1.27 ± 0.09	0.904 [0.847, 0.961]	30/30
Disturbance-window RMSE (rad/s)	1.45 ± 0.21	0.29 ± 0.02	1.160 [1.087, 1.234]	30/30
Maximum disturbance-window error (rad/s)	2.82 ± 0.43	1.28 ± 0.28	1.539 [1.439, 1.639]	30/30
RMS current (A)	4.54 ± 0.33	3.13 ± 0.30	1.413 [1.293, 1.533]	30/30
Peak current (A)	16.75 ± 2.13	15.98 ± 1.74	0.775 [0.397, 1.153]	27/30
Peak voltage (V)	90.53 ± 6.15	97.94 ± 6.69	-7.413 [-8.150, -6.675]	0/30

Figure 7 shows the paired values for speed RMSE, disturbance-window RMSE, and RMS current. Every line slopes downward from adaptive to proposed control. The improvement is therefore repeated across all 30 uncertainty and noise realizations.

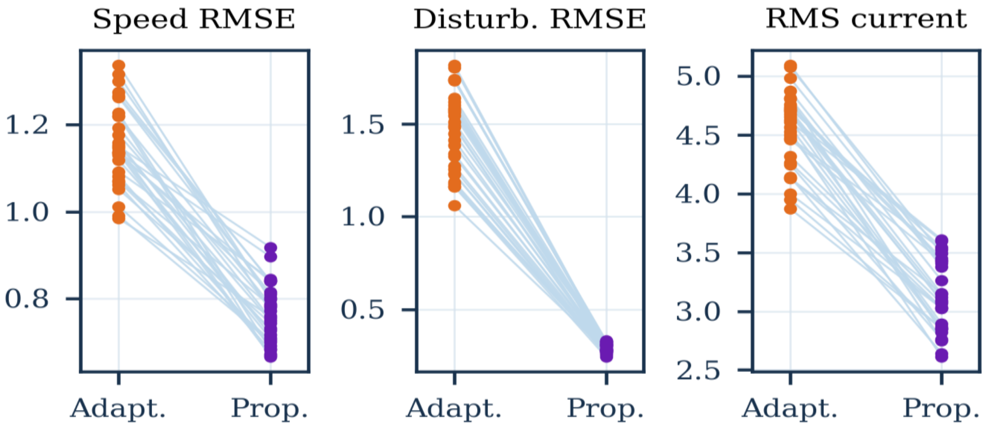

Figure 7: Paired adaptive-to-proposed values for all 30 Monte Carlo runs.

All runs of the proposed controller remained within the current and voltage limits. The highest speed RMSE recorded was 0.9185 rad/s, while the highest disturbance RMSE was 0.3329 rad/s. Peak current and voltage reached 19.901 A and 111.44 V, respectively. The peak value of the disturbance was estimated at 30.02 V, leaving 1.98 V of unused reserve, and the event logic performed exactly as intended.

Under normal operation, 94.24% of the current NIS values and 94.45% of the three-state NEES values stayed within the 95% confidence limits. Their means were also close to the expected values, showing that the UKF filter covariance was reasonably calibrated.

The proposed controller found a feasible solution for all 90,000 optimization samples. Fixed NMPC failed once, whereas adaptive NMPC reached its iteration limit 191 times. The same performance trend remained when the comparison was limited to the 21 runs without an adaptive-NMPC failure. Mean solution times were 79.25 ms for fixed NMPC, 58.72 ms for adaptive NMPC, and 52.33 ms for the proposed method. These times are far above the 1 ms sampling period, so the present MATLAB/CasADi implementation is suitable only for offline analysis. Real-time operation would require a faster solver, a shorter horizon, or moving blocking. Another option is to run NMPC at a slower supervisory rate.

Conclusion

This study developed an event-governed estimation and control method for a PMSM to prevent fast inverter-voltage disturbances from being interpreted as changes in flux linkage or load torque. When the current innovation indicated a possible event, the guarded two-time-scale UKF retained the last reliable estimates of these slow quantities. The adaptive NMPC used the same event decision and did not apply cancellation until the disturbance was confirmed. A tightened voltage constraint reserved sufficient inverter margin for the corrective voltage.

Estimator replay showed that preserving the slow-state means mainly prevented voltage errors from being absorbed into the flux-linkage and load-torque estimates. After separating this estimation effect, the comparison of operation with and without cancellation showed that the corrective voltage improved speed tracking. The sensitivity calculation supported these findings by showing that voltage and flux-linkage errors produce very similar current responses near constant speed, making them difficult to estimate separately.

The consistency of the results was examined through 30 paired Monte Carlo trials. Compared with the cancellation-disabled case, the proposed method reduced the mean speed RMSE by 33.8%, the disturbance-window RMSE by 79.8%, and the RMS current by 31.1%. The corrective action increased peak voltage by 8.2%, but it did not violate any current or voltage limits. These results indicate that the proposed coordination improves disturbance attribution and speed tracking under the tested simulation conditions.

Future work will test the method on an experimental PMSM drive, including inverter switching effects, and investigate a faster NMPC solver that can meet the required sampling period.

Compliance with ethical standards

Disclosure of conflict of interest

The authors declare that they have no conflict of interest.

References

[1] T. Li, X. Sun, G. Lei, Y. Guo, Z. Yang, and J. Zhu, "Finite-control-set model predictive control of permanent magnet synchronous motor drive systems—An overview," *IEEE/CAA Journal of Automatica Sinica*, vol. 9, no. 12, pp. 2087-2105, 2022. doi: 10.1109/JAS.2022.105851.

[2] M. Preindl and S. Bolognani, "Model predictive direct speed control with finite control set of PMSM drive systems," *IEEE Transactions on Power Electronics*, vol. 28, no. 2, pp. 1007-1015, 2012. doi: 10.1109/TPEL.2012.2204277

[3] P. Kakosimos and H. Abu-Rub, "Predictive speed control with short prediction horizon for permanent magnet synchronous motor drives," *IEEE Transactions on Power Electronics*, vol. 33, no. 3, pp. 2740-2750, 2017. doi: 10.1109/TPEL.2017.2697971.

[4] X. Zhang, L. Zhang, and Y. Zhang, "Model predictive current control for PMSM drives with parameter robustness improvement," *IEEE Transactions on Power Electronics*, vol. 34, no. 2, pp. 1645-1657, 2018. doi: 10.1109/TPEL.2018.2835835

[5] Z.-Q. Zhu, D. Liang, and K. Liu, "Online parameter estimation for permanent magnet synchronous machines: An overview," *Ieee Access*, vol. 9, pp. 59059-59084, 2021. doi : 10.1109/ACCESS.2021.3072959

[6] K. Liu and Z.-Q. Zhu, "Online estimation of the rotor flux linkage and voltage-source inverter nonlinearity in permanent magnet synchronous machine drives," *IEEE Transactions on Power Electronics*, vol. 29, no. 1, pp. 418-427, 2013. doi: 10.1109/TPEL.2013.2252024.

[7] K. Horváth, "Position sensorless extended and unscented Kalman filters with permanent magnet flux linkage and load torque estimation for surface-mounted PMSM," *Automatika*, vol. 65, pp. 1201-1212, 2024-05-22 2024, doi: 10.1080/00051144.2024.2354643.

[8] D. Janiszewski, "Sensorless Model Predictive Control of Permanent Magnet Synchronous Motors Using an Unscented Kalman Filter," *Energies*, 2024-05-16 2024, doi: 10.3390/en17102387.

[9] A. P. Yadav, M. Davoodi, N. R. Gans, and A. Davoudi, "Partial-update Kalman filter for permanent magnet synchronous motor estimates under intermittent data," *IEEE Access*, vol. 10, pp. 67305-67315, 2022. doi:10.1109/ACCESS.2022.3185744

[10] Y. Zhang, J. Jin, and L. Huang, "Model-free predictive current control of PMSM drives based on extended state observer using ultralocal model," *IEEE Transactions on Industrial Electronics*, vol. 68, no. 2, pp. 993-1003, 2020. doi:10.1109/ICEMS.2019.8922216.

[11] X. Lin, J. Liu, Z. Liu, Y. Gao, L. Peretti, and L. Wu, "Model-Free Current Predictive Control for PMSMs With Ultralocal Model Employing Fixed-Time Observer and Extremum-Seeking Method," *IEEE Transactions on Power Electronics*, vol. 40, pp. 10682-10693, 2025-08-01 2025, doi: 10.1109/tpel.2025.3553685.

[12] Z. Zhu, X. Wei, R. Han, C. Liu, and Z. Zhang, "Double-Vector Model-Free Predictive Current Control for PMSMs With Influence Rejection of DC Voltage Mismatch," *IEEE Transactions on Transportation Electrification*, vol. 11, pp. 6143-6153, 2025-04-01 2025, doi: 10.1109/tte.2024.3498950.

[13] X. Sun, Z. Huang, Z. Yang, G. Lei, and T. Li, "Improved Model-Free Predictive Current Control for Suppressing Inverter Nonlinearity and Parametric Time-Varying of PMSM Drive Systems," *IEEE Transactions on Industrial Electronics*, vol. 72, pp. 9866-9875, 2025-10-01 2025, doi: 10.1109/tie.2024.3488276 .

[14] L. Gao and F. Chai, "Model Predictive Direct Speed Control of Permanent-Magnet Synchronous Motors with Voltage Error Compensation," *Energies*, 2023-07-03 2023, doi: 10.3390/en16135128.

[15] Z. Zhang, Y. Liu, X. Liang, H. Guo, and X. Zhuang, "Robust Model Predictive Current Control of PMSM Based on Nonlinear Extended State Observer," *IEEE Journal of Emerging and Selected Topics in Power Electronics*, vol. 11, pp. 862-873, 2023-02-01 2023, doi:10.1109/JESTPE.2022.3192064.

[16] L. Gao, G. Zhang, X. Lv, Y. Wang, and Z. Shi, "A Finite-Time Extended State Observer with Prediction Error Compensation for PMSM Control," *Comput.*, vol. 13, p. 247, 2025-10-20 2025, doi: 10.3390/computation13100247.

[17] X. Zhang, Y. Cao, and C. Zhang, "Model Predictive Voltage Control for PMSM System With Low Parameter Sensitivity," *IEEE Transactions on Industrial Electronics*, vol. 71, pp. 13601-13613, 2024-11-01 2024, **DOI:** 10.1109/TIE.2024.3376830.

[18] Z. Su, X. Sun, G. Lei, M. Yao, and L. Zhang, "Augmented Continuous-Control-Set Model Predictive Current Control for Dual Three-Phase PMSM Drives," *IEEE/ASME Transactions on Mechatronics*, vol. 30, pp. 2367-2378, 2025-06-01 2025, **DOI:** 10.1109/TMECH.2024.3446598

[19] S. Zhu *et al.*, "Nonlinear Flux Linkage Observer with Model Reference Adaptive System for Improved Permanent Magnet Synchronous Motor Control," *Actuators*, 2024-10-06 2024, doi: 10.3390/act13100403.

[20] H. Djouadi, K. Ouari, Y. Belkhier, and H. Lehouche, "Real-Time HIL Simulation of Nonlinear Generalized Model Predictive-Based High-Order SMC for Permanent Magnet Synchronous Machine Drive," *International Transactions on Electrical Energy Systems*, 2024-03-07 2024, doi: 10.1155/2024/5536555.

[21] T. Nguyen, H. Tran, T. H. Nguyen, and J. Jeon, "Recurrent Neural Network-Based Robust Adaptive Model Predictive Speed Control for PMSM With Parameter Mismatch," *IEEE Transactions on Industrial Electronics*, vol. 70, pp. 6219-6228, 2023-06-01 2023, doi: 10.1109/tie.2022.3198255.
[22] Y. Luo, K. Yang, and Y. Zheng, "Luenberger Observer-Based Model Predictive Control for Six-Phase PMSM Motor With Localization Error Compensation," *IEEE Transactions on Industrial Electronics*, vol. 70, pp. 10800-10810, 2023, doi: 10.1109/tie.2022.3229340.
[23] M. Ismail, W. Xu, J. Ge, Y. Tang, A. Junejo, and M. Hussien, "Adaptive Linear Predictive Model of an Improved Predictive Control of Permanent Magnet Synchronous Motor Over Different Speed Regions," *IEEE Transactions on Power Electronics*, vol. 37, pp. 15338-15355, 2022-12-01 2022, doi: 10.1109/tpel.2022.3194839.
[24] H. Li, S. Li, and Y. Yan, "Disturbance observer based MPC for PMSM with multiple disturbances," in *2023 IEEE International Conference on Predictive Control of Electrical Drives and Power Electronics (PRECEDE)*, 2023: IEEE, pp. 1-6. doi: 10.1109/PRECEDE57319.2023.10174295
[25] J. Wang, Z. Chen, R. Wang, Y. Li, J. Yang, and J. Rodríguez, "Disturbance pre-estimation based receding horizon predictive control for PMSM drives," *IEEE Transactions on Power Electronics*, vol. 40, no. 10, pp. 14638-14650, 2025 doi: 10.1109/TPEL.2025.3577447
[26] R. Zu, N. Jiang, Y. Huang, and D. Xu, "Robust Predictive Control of PMSM via Dual-Loop Parameter-Disturbance Adaptation," *IEEE Access*, vol. 13, pp. 98759-98770, 2025. doi: 10.1109/ACCESS.2025.3577056
[27] S. Julier and J. Uhlmann, "Unscented filtering and nonlinear estimation," *Proceedings of the IEEE*, vol. 92, pp. 401-422, 2004-11-08 2004, doi: 10.1109/JPROC.2003.823141.
[28] E. A. Wan and R. Van Der Merwe, "The unscented Kalman filter for nonlinear estimation," in *Proceedings of the IEEE 2000 adaptive systems for signal processing, communications, and control symposium (Cat. No. 00EX373)*, 2000: Ieee, pp. 153-158. doi: 10.1109/ASSPCC.2000.882463
[29] F. Gao, P. Zhang, Z. Yin, Y. Yang, and Y. Ren, "Robust sensorless control of synchronous reluctance motor drives for electric vehicles via adaptive Kalman filtering and online resistance identification," *eTransportation*, p. 100601, 2026. doi: 10.1016/j.etran.2026.100601
[30] D. Hou, Y. Sun, V. Dinavahi, and Y. Wang, "Adaptive two-stage unscented Kalman filter for dynamic state estimation of synchronous generator under cyber attacks against measurements," *Journal of Modern Power Systems and Clean Energy*, vol. 12, no. 5, pp. 1408-1418, 2024. doi: 10.35833/MPCE.2023.000352
[31] H. Xie, L. Dai, Y. Lu, and Y. Xia, "Disturbance rejection MPC framework for input-affine nonlinear systems," *IEEE Transactions on Automatic Control*, vol. 67, no. 12, pp. 6595-6610, 2021. doi: 10.1109/TAC.2021.3133376
[32] D. Q. Mayne, M. M. Seron, and S. V. Raković, "Robust model predictive control of constrained linear systems with bounded disturbances," *Automatica*, vol. 41, no. 2, pp. 219-224, 2005. doi: 10.1016/j.automatica.2004.08.019
[33] J. Köhler, R. Soloperto, M. A. Müller, and F. Allgöwer, "A computationally efficient robust model predictive control framework for uncertain nonlinear systems," *IEEE Transactions on Automatic Control*, vol. 66, no. 2, pp. 794-801, 2020. doi: 10.1109/TAC.2020.2982585
[34] P. Pillay and R. Krishnan, "Modeling, simulation, and analysis of permanent-magnet motor drives. I. The permanent-magnet synchronous motor drive," *IEEE Transactions on industry applications*, vol. 25, no. 2, pp. 265-273, 1989. doi: 10.1109/28.25541
[35] E. Hairer and G. Wanner, *Solving Ordinary Differential Equations II*. 1996. doi: 10.1007/978-3-642-05221-7
[36] Y. Bar-Shalom, X. R. Li, and T. Kirubarajan, *Estimation with applications to tracking and navigation: theory algorithms and software*. John Wiley & Sons, 2001. doi: 10.1002/0471221279
[37] W. Bich, M. G. Cox, and P. M. Harris, "Evolution of the 'Guide to the Expression of Uncertainty in Measurement'," *Metrologia*, vol. 43, no. 4, pp. S161-S166, 2006. doi: 10.1088/0026-1394/43/4/S01
[38] J. B. Rawlings, D. Q. Mayne, and M. M. Diehl, "Model predictive control: theory, computation, and design," *(book)*, 2020. ISBN 978-0-9759377-5-4
[39] J. A. Andersson, J. Gillis, G. Horn, J. B. Rawlings, and M. Diehl, "CasADi: a software framework for nonlinear optimization and optimal control: JAE Andersson et al," *Mathematical Programming Computation*, vol. 11, no. 1, pp. 1-36, 2019. doi: 10.1007/s12532-018-0139-4
[40] A. Wächter and L. T. Biegler, "On the implementation of an interior-point filter line-search algorithm for large-scale nonlinear programming," *Mathematical programming*, vol. 106, no. 1, pp. 25-57, 2006. doi: 10.1007/s10107-004-0559-y

